Simulations of Turbulent Momentum and Scalar Transport in Non-Reacting Confined Swirling Coaxial Jets

Tsan-Hsing Shih
Ohio Aerospace Institute
Cleveland Ohio 44142 USA

Nan-Suey Liu and Jeffrey P. Mode
NASA Glenn Research Center
Cleveland Ohio 44135 USA

Abstract

This paper presents the numerical simulations of confined three-dimensional coaxial water jets. The objectives are to validate the newly proposed nonlinear turbulence models of momentum and scalar transport, and to evaluate the newly introduced scalar APDF and DWFDF equation along with its Eulerian implementation in the National Combustion Code (NCC). Simulations conducted include the steady RANS, the unsteady RANS (URANS), and the time-filtered Navier-Stokes (TFNS); both without and with invoking the APDF or DWFDF equation. When the APDF (ensemble averaged probability density function) or DWFDF (density weighted filtered density function) equation is invoked, the simulations are of a hybrid nature, i.e., the transport equations of energy and species are replaced by the APDF or DWFDF equation. Results of simulations are compared with the available experimental data. Some positive impacts of the nonlinear turbulence models and the Eulerian scalar APDF and DWFDF approach are observed.

Introduction

In this study we have focused on two subjects. The first one is to validate the newly proposed nonlinear models of turbulent momentum and scalar transport implemented in the NCC code[1] using the experimental data from confined swirling coaxial water jets[2], and assess the performance of the nonlinear scalar flux model relative to the linear scalar flux model. The second one is to validate the newly introduced scalar APDF[3] and DWFDF[4] equations and their Eulerian implementations in the NCC code using the same experimental data. Both validations have been carried out with three types of numerical simulation approaches. The first two approaches are the steady RANS and the unsteady RANS (URANS). The third one is the time filtered Navier-Stokes (TFNS[5, 6]) approach.

The experimental study provided flow structures that resemble those often found in a gas turbine combustors, for example, center swirling recirculation near the front of combustor, massive swirled separations at the front corners, strong swirling flow extended all the way to the exit of combustor, and significant changes of concentration in the radial direction at the front of combustor, etc. The detailed experimental data on the velocity and scalar concentration distributions are available for validating the turbulence models and evaluating the numerical simulation approaches. Since water was used in the experiments and NCC solves the compressible Navier-Stokes equations supplemented by the equation of state for ideal gas, the water flow experiment was converted to its corresponding air flow simulation according to the Reynolds number similarity rule under the condition of low speed. The results of air flow simulations were then rescaled back to their water flow counterparts and compared with the experimental data.

The turbulence models for momentum and scalar transport validated in the current simulations are listed in the next Section under the title *"Linear model versus nonlinear model"*. The APDF and DWFDF equation invoked in the hybrid approach of RANS/APDF, URANS/APDF and TFNS/DWFDF simulations are listed under the title *"Scalar APDF and DWFDF equation"*.

More detailed results of validations of the turbulence models are presented in NASA/TM—2014-218134. The results obtained from the linear scalar flux model and those from the nonlinear scalar flux model in all three types of simulations (RANS, URANS and TFNS) are compared with the available experimental

data, including the results obtained by invoking the APDF and DWFDF equation. Note, the simulations mentioned in the later are of hybrid nature, i.e. the velocity field is solved by the continuity and momentum equations, but the transport equations of energy and species are replaced by the equation of APDF or DWFDF, and the APDF or DWDFD equation is solved by an Eulerian Monte Carlo particle method[7]. In the Section "Numerical results of simulations", we briefly describe the above mentioned numerical validations compared with experimental data. In addition, comparison of the RANS results between using a conventional standard $k-\varepsilon$ model and using the present non-linear $k-\varepsilon$ model is also presented to demonstrate the improvements due to the current nonlinear models.

Turbulence models and Scalar PDF equation

The models for turbulent stress tensor τ_{ij} and scalar flux Θ_i as well as the scalar APDF and DWFDF equation employed in the current simulations are presented in this section.

Linear model versus nonlinear model

Linear models of turbulent stresses and scalar fluxes

Based on the Boussinesq approximation of the linear relationship between the turbulent stress and the strain rate of flow field, the linear model of turbulent stress is formulated as

$$\tau_{ij} - \frac{1}{3}\delta_{ij}\tau_{kk} = -2 f C_\mu \bar{\rho} \frac{k^2}{\varepsilon}\left(\tilde{S}_{ij} - \delta_{ij}\tilde{S}_{kk}/3\right)$$

Similarly, the linear model of turbulent scalar flux is formulated as

$$\Theta_i = -\vartheta_T \frac{\partial \bar{\rho}\tilde{\theta}}{\partial x_i}$$

Nonlinear models of turbulent stresses and scalar fluxes

A general constitutive relationship between the turbulent stresses τ_{ij} and the strain rate of flow field $\tilde{S}_{ij}$, $\tilde{\Omega}_{ij}$ suggests (Ref.[6, 8])

$$\tau_{ij} - \frac{1}{3}\delta_{ij}\tau_{kk} = -2 f C_\mu \bar{\rho}\frac{k^2}{\varepsilon}\left(\tilde{S}_{ij} - \delta_{ij}\tilde{S}_{kk}/3\right)$$

$$- A_3 f \bar{\rho}\frac{k^3}{\varepsilon^2}\left(\tilde{S}_{ik}\tilde{\Omega}_{kj} - \tilde{\Omega}_{ik}\tilde{S}_{kj}\right)$$

$$+ 2A_5 f \bar{\rho}\frac{k^4}{\varepsilon^3}[\tilde{\Omega}_{ik}\tilde{S}_{kj}^2 - \tilde{S}_{ik}^2\tilde{\Omega}_{kj} + \tilde{\Omega}_{ik}\tilde{S}_{km}\tilde{\Omega}_{mj}$$

$$- \tilde{\Omega}_{kl}\tilde{S}_{lm}\tilde{\Omega}_{mk}\delta_{ij}/3 + II_s(\tilde{S}_{ij} - \delta_{ij}\tilde{S}_{kk}/3)]$$

where

$$\tilde{S}_{ij} = \left(U_{i,j} + U_{j,i}\right)/2 ,$$

$$\tilde{\Omega}_{ij} = \left(U_{i,j} - U_{j,i}\right)/2 ,$$

$$II_s = \left(\tilde{S}_{kk}\tilde{S}_{mm} - \tilde{S}_{kl}\tilde{S}_{lk}\right)/2$$

The model coefficients C_μ, A_3 and A_5 are constrained by the realizability condition and the rapid distortion theory. They are formulated as (see Ref.[9]):

$$C_\mu = \frac{1}{4.0 + A_s \dfrac{k}{\varepsilon}U^*} ,$$

$$A_3 = \frac{\sqrt{1.0 - A_s^2 C_\mu^2 \left(\dfrac{k}{\varepsilon}S^*\right)^2}}{0.5 + 1.5\dfrac{k^2}{\varepsilon^2}\Omega^* S^*} ,$$

$$A_5 = \frac{1.6 C_\mu \bar{\rho}\dfrac{k^2}{\varepsilon}}{\bar{\rho}\dfrac{k^4}{\varepsilon^3}\dfrac{7S^*S^* + \Omega^*\Omega^*}{4}}$$

in which,

$$A_s = \sqrt{6}\cos\varphi, \quad \varphi = \frac{1}{3}\arccos\left(\sqrt{6}W^*\right),$$

$$W^* = \frac{S_{ij}^*S_{jk}^*S_{ki}^*}{(S^*)^3},$$

$$U^* = \sqrt{(S^*)^2 + (\Omega^*)^2}, \quad S^* = \sqrt{S_{ij}^*S_{ij}^*},$$

$$\Omega^* = \sqrt{\tilde{\Omega}_{ij}\tilde{\Omega}_{ij}}, \quad S_{ij}^* = \tilde{S}_{ij} - \frac{1}{3}\delta_{ij}\tilde{S}_{kk}$$

The coefficient f is a function of the filtering resolution control parameter (RCP) that is defined as a ratio of the time filter width Δ_T to a global integral time scale of the flow T : RCP $= \Delta_T / T$ and

$$f\left(\frac{\Delta_T}{T}\right) \approx 2\left(\frac{\Delta_T}{T}\right) - \left(\frac{\Delta_T}{T}\right)^2$$

As discussed in Ref.[6], RCP may be viewed as a percentage measure of the unresolved subscale turbulent kinetic energy relative to the total turbulent kinetic energy. Therefore, the value of RCP and the coefficient f are always between 0 and 1, and $f = 1.0$ in RANS and URANS simulations, $f < 1.0$ in TFNS.

Similarly, the nonlinear model for scalar fluxes is formulated as (Ref.[10]),

$$\Theta_i = -\vartheta_T \frac{\partial \bar{\rho}\,\tilde{\theta}}{\partial x_i} - \vartheta_T \frac{k}{\varepsilon}\left(c_1 \tilde{S}_{ij} + c_2 \tilde{\Omega}_{ij}\right)\frac{\partial \bar{\rho}\,\tilde{\theta}}{\partial x_j}$$

Where ϑ_T denotes the turbulent diffusivity for the corresponding scalar quantity θ. It is often approximated by $\vartheta_T = \nu_T / \mathrm{Pr}^\theta$, where Pr^θ represents the turbulent Prandtl number or Schmidt number depending on whether the scalar quantity $\tilde{\theta}$ is the internal energy $\tilde{e}$ or the species mass fraction $\tilde{\Phi}_m$. The turbulent eddy viscosity is defined as $\nu_T = f \cdot C_\mu \cdot k^2 / \varepsilon$. The coefficients c_1 and c_2 in the current simulations are set to be $c_1 = c_2 = -0.24$.

Model equations of turbulent kinetic energy and its dissipation rate

The (subscale or total) turbulent kinetic energy k and its dissipation rate ε will be determined from the following model equations:

$$\frac{\partial}{\partial t}\bar{\rho}k + \frac{\partial}{\partial x_i}\bar{\rho}\tilde{u}_i k = \frac{\partial}{\partial x_i}\left[\left(\mu + \mu_T\right)\frac{\partial}{\partial x_i}k\right]$$
$$- \tau_{ij}\tilde{s}_{ij} - \bar{\rho}\varepsilon$$

$$\frac{\partial}{\partial t}\bar{\rho}\varepsilon + \frac{\partial}{\partial x_i}\bar{\rho}\tilde{u}_i \varepsilon = \frac{\partial}{\partial x_i}\left[\left(\mu + \mu_T\right)\frac{\partial}{\partial x_i}\varepsilon\right]$$
$$- C_{\varepsilon 1}\tau_{ij}\tilde{s}_{ij}\frac{\varepsilon}{k} - C_{\varepsilon 2}\frac{\bar{\rho}\varepsilon^2}{k}$$

where $C_{\varepsilon 1}$ and $C_{\varepsilon 2}$ are model coefficients. We have adopted the commonly used values of $C_{e1} = 1.45$ and $C_{e2} = 1.92$ in the present simulations.

Scalar APDF and DWFDF equation

The transport equation for the scalar APDF or DWFDF, $F_\Phi(\psi; x, t)$, can be written as (Ref.[3, 4])

$$\frac{\partial F_\Phi}{\partial t} + \frac{\partial\left(U_i F_\Phi\right)}{\partial x_i} = \left\{\frac{\partial}{\partial x_i}\left(\left(\Gamma^{(m)} + \Gamma_T^{(m)}\right)\frac{\partial F_\Phi}{\partial x_i}\right)\right\}$$
$$- \frac{\partial}{\partial \psi_k}\left(F_\Phi \cdot S_k(\psi)\right) + f \cdot \frac{\partial}{\partial \psi_k}\left(\psi_k \frac{1}{\tau} F_\Phi\right),$$
$$k = 1, 2, \cdots, M+1$$

where

$$\frac{1}{\tau} \approx \sqrt{S_{ij} S_{ij} + \Omega_{ij}\Omega_{ij}}\,, \qquad \tau \geq \sqrt{(\nu + \nu_T)/\varepsilon}$$

Results of numerical simulations

Figure 1 shows the computational domain and the unstructured mesh grid (Ref.[11]), which consists of 849,189 tetrahedral elements having 152,555 nodes. Based on the Reynolds number similarity, the case of swirling coaxial water jets was scaled to the case of swirling coaxial air jets, to enable use of the NCC code to simulate this low Mach number flow. The water dye concentration was represented by the mass fraction of the dyed air. There are two inlet boundaries, one is for the inner tube, at which the velocity, temperature and density were specified: 25.87 m/s, 300 K, and 1.1774 kg/m3; another one is for the annulus, at which radial profile was specified. The annular air passes through 8 swirlers resulting into an annular swirling jet dumped into a suddenly expanded chamber and mixed with the inner dyed air jet. Complex flow features exist in the chamber: shear layers, massive separations near the front corner of the chamber and the center recirculation, etc. (see Figure 2). At the exit of the chamber, the pressure of 1.0 atm. was specified for RANS and URANS simulations, whereas an unsteady convective boundary condition was specified for TFNS simulations.
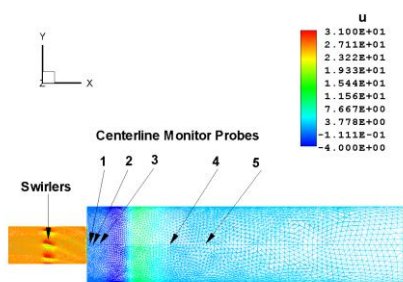
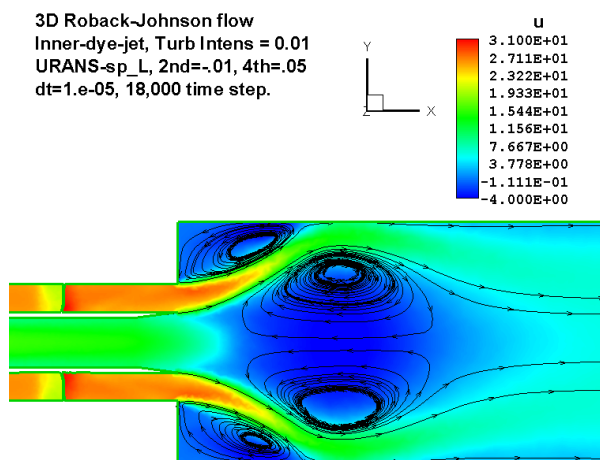**Figure 1   Computational domain and mesh grid.**

Figure 2 Flow structures in the center X-Y plane.

A complete set of numerical simulations are presented in NASA/TM-2014-218134 through six groups, each one focuses on a different simulation approach: RANS, URANS, TFNS, RANS/APDF, URANS/APDF, and TFNS/DWFDF.

In the first three simulation groups, the main interest is the turbulent scalar flux models, i.e., the performance of nonlinear scalar flux model versus the performance of linear scalar flux model; hence the turbulent stress model used in these simulations remains the same nonlinear model that has already been validated in the past studies. In this study, the experimental data for dye concentration is used to validate the newly proposed nonlinear scalar flux model.

In the second three simulation groups, the main

interest is the hybrid approach, in which the scalar APDF or DWFDF equation is invoked to replace the transport equations of energy and species, and an Eulerian solver for the APDF or DWFDF equation is employed. The numerical results from the hybrid RANS/APDF, URANS/APDF and TFNS/DWFDF approaches are compared with the experimental data. In this paper, we only present a few results from each of above simulation groups.
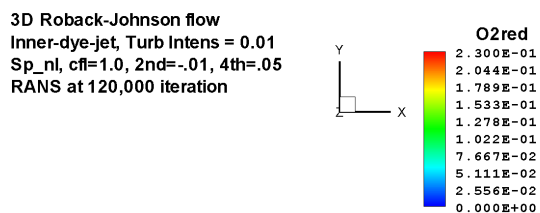
Scalar flux model: linear vs. nonlinear
RANS, URANS and TFNS simulations have been performed using both linear and nonlinear scalar flux models to examine their effects on all turbulent flow variables and concentration distribution.

For RANS simulations, there are no noticeable differences between simulations using the linear scalar flux model and nonlinear scalar flux model, as shown in following two contour plots:
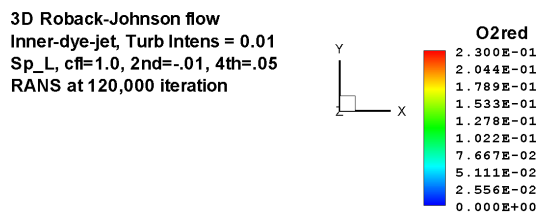

Dyed air concentration contour at center plane from linear scalar flux model.


Dyed air concentration contour at center plane from nonlinear scalar flux model.

For URANS simulations, there is also very little difference observed in the numerical results due to the application of linear and nonlinear scalar flux

models. The similarity in results are shown, for example, in following two figures (the inner jet concentration along the centerline and the radial profile at the downstream x = 51 mm):
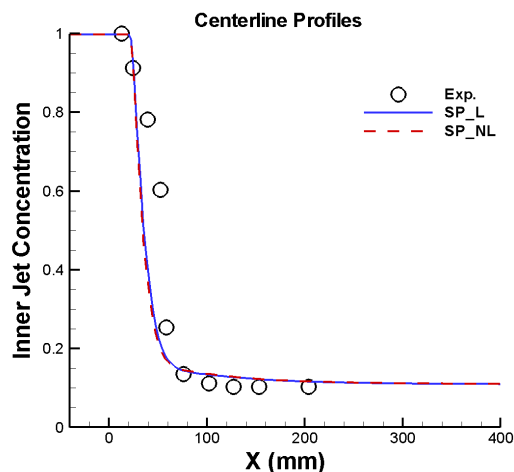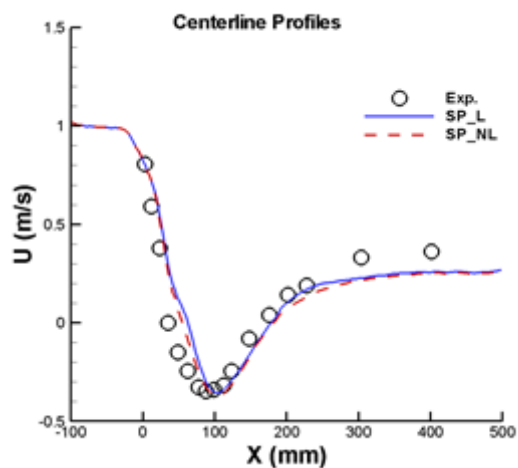

**URANS: Concentration along the centerline**
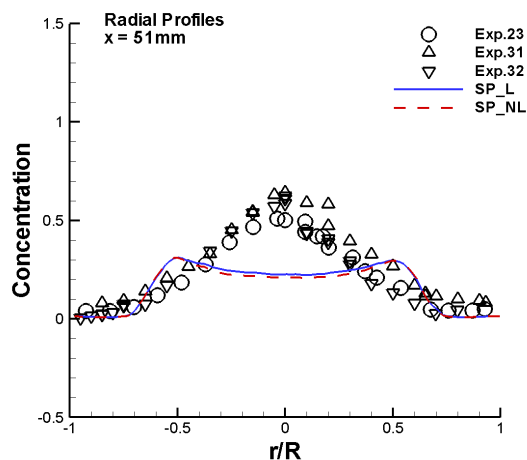
URANS: Concentration at a downstream location

For very large eddy simulations using TFNS, noticeable but not significant differences have been observed. These can typically be seen from the following two figures: the inner jet concentration along the centerline and the radial profile at the downstream location x = 51 mm.

TFNS: Mean axial velocity along the centerline
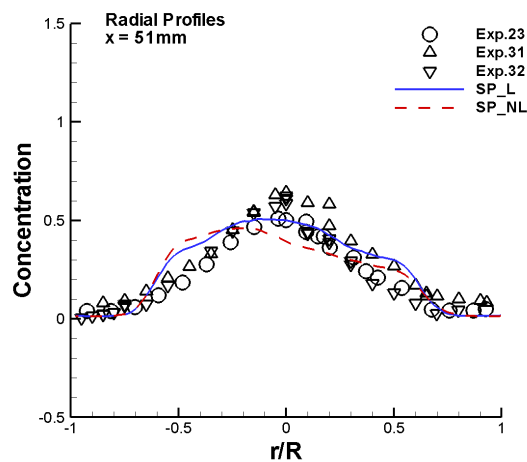
TFNS: Mean concentration at a downstream location

Hybrid Approaches: RANS/APDF, URANS/APDF and TFNS/DWFDF

These hybrid approaches are performed and compared with the pure RANS, URANS and TFNS simulations to examine the possible benefits from the invoking the newly proposed PDF equations. The following characteristics have been observed.

RANS/APDF simulations produce the same results as the pure RANS simulations, but with faster numerical convergence rates. Typical concentration results for RANS and RANS/APDF are shown below:
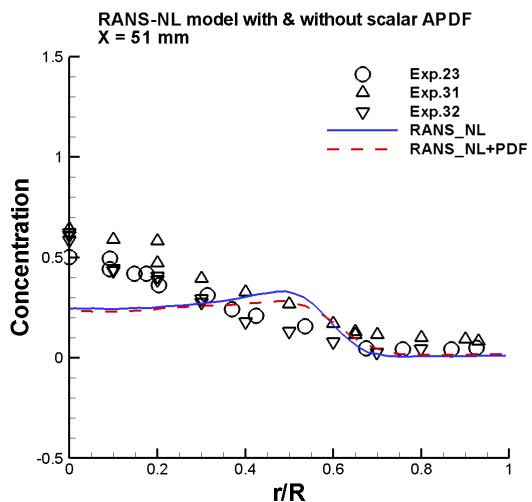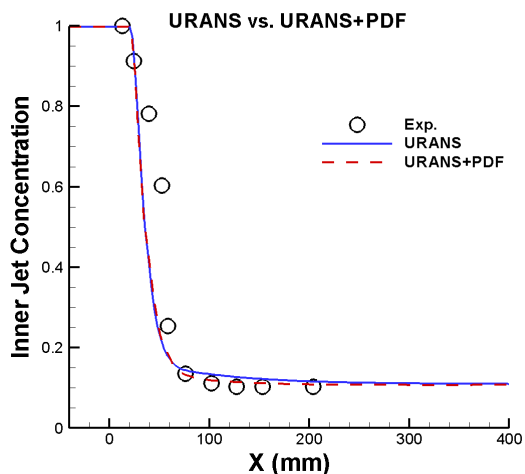
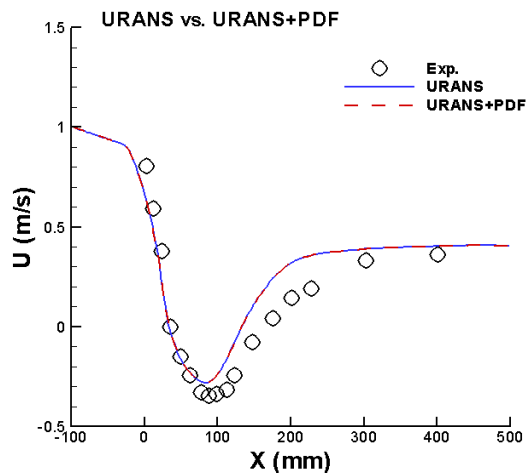**Radial distributions of concentration at downstream location x = 51 mm**
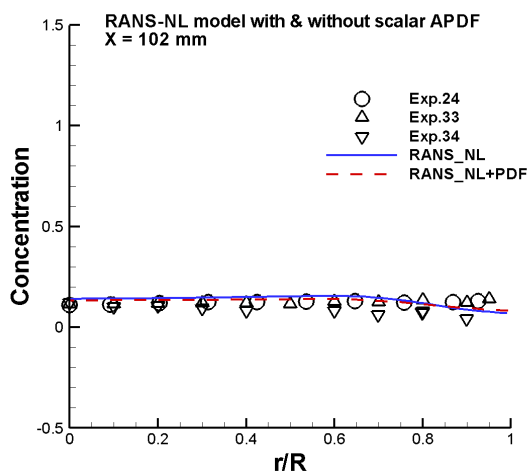
Radial distributions of concentration at downstream location x = 102 mm.

URANS/APDF simulations produce the same or better results compared to pure URANS simulations:

**Centerline distributions of concentration**

Centerline distributions of axial velocity.

TFNS/DWFDF simulations are superior in terms of both numerical efficiency and accuracy compared to pure TFNS simulations. The hybrid very large eddy simulations (TFNS/DWFDF) converge much faster and more stable compared to pure TFNS simulations.
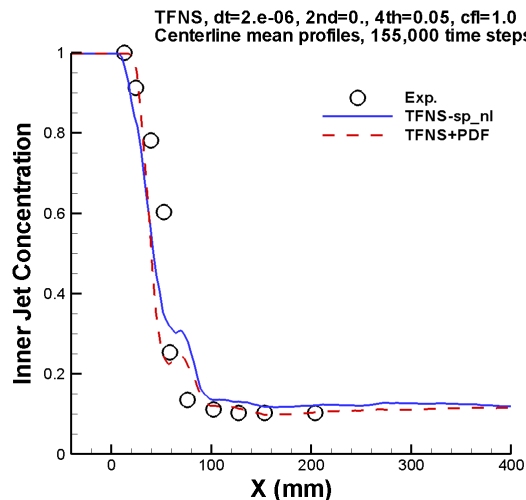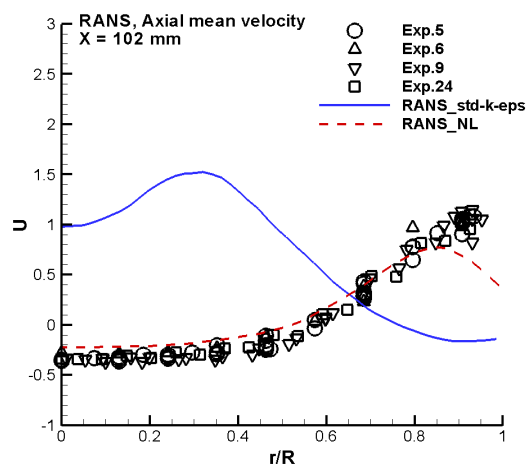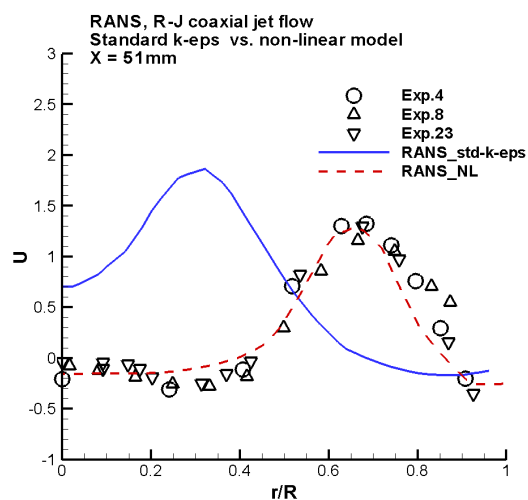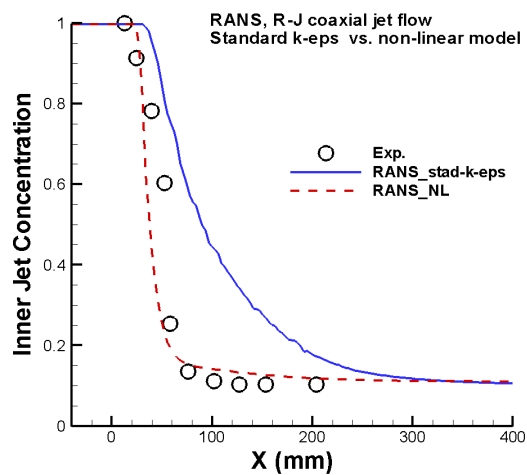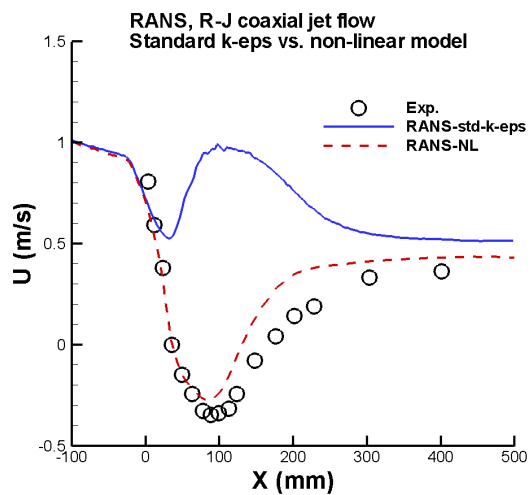

Mean concentration along the centline
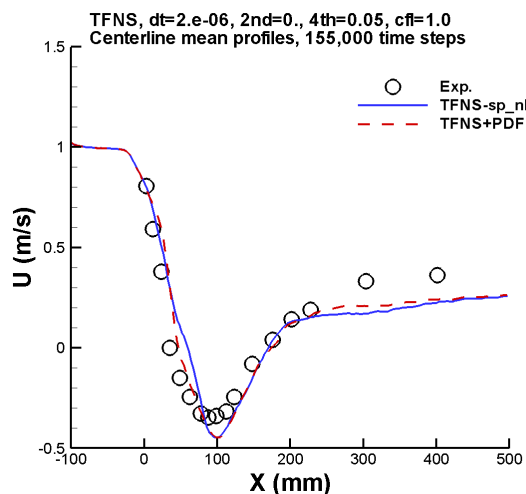
Mean axial velocity along the centline

Appendix: Simulations with standard $k - \varepsilon$ model versus non-linear $k - \varepsilon$ model

Finally, a comparison of the RANS results using a conventional standard $k - \varepsilon$ model and the present non-linear $k - \varepsilon$ model is presented to demonstrate the improvements due to the current nonlinear model of turbulent momentum transfer.

RANS, R-J coaxial jet flow
Standard k-eps vs. non-linear model

RANS, R-J coaxial jet flow
Standard k-eps vs. non-linear model

RANS, R-J coaxial jet flow
Standard k-eps vs. non-linear model
X = 51mm

RANS, Axial mean velocity
X = 102 mm

Conclusions

Two groups of validations have been performed using the experiments of a confined swirling coaxial water jets. The first validation group focuses on the turbulent scalar flux model to explore the performance of the linear formulation versus the nonlinear formulation. Simulations conducted for this group include RANS, URANS and TFNS. The second group focuses on the hybrid approach to explore the performance of the newly introduced APDF and DWFDF equation and the Eulerian solver for this equation. Simulations conducted for this group include RANS/APDF, URANS/APDF and TFNS/DWFDF.

Regarding to the scalar flux model, the linear and nonlinear model have the same behave in RANS and URANS simulations. Their respective results shown in various contour plots and profiles at different downstream locations are almost identical and in reasonable agreement with the experimental data. In the case of TFNS simulations, the differences in results for the linear and nonlinear models are small but noticeable. Furthermore, the TFNS results demonstrate significant improvements over their RANS and URANS counter parts, when compared with the experimental data.

Regarding the hybrid approach, the results of RANS/APDF, URANS/APDF and TFNS/DWFDF simulations show that these approaches are very close to their respective RANS, URANS and TFNS counterpart. Our current experience indicates that the hybrid approach is more robust for both steady and unsteady simulations with faster numerical convergence compared to its respective approach of pure RANS, URANS and TFNS.

Acknowledgemens

References

Liu, N.-S., "On the Comprehensive Modeling and Simulation of Combustion Systems," AIAA-2001-0805, January 2001.

Roback, R. and Johnson, B. V., "Mass and Momentum Turbulent Transport Experiments with Confined Swirling Coaxial Jets," NASA CR 168252, August 1983.

Shih, T.-H. and Liu, N.-S., "Ensemble Averaged Probability Density Function (APDF) Equations for Compressible Turbulent Reacting Flows," NASA/TM-2012-217677, August, 2012.

Shih, T.-H. and Liu, N.-S., "Density Weighted FDF Equations for Simulations of Turbulent Reacting Flows," NASA/TM-2011-217012, May 2011.

Liu, N.-S. and Shih, T.-H., "Turbulence Modeling for Very Large-Eddy Simulation", *AIAA Journal,* Vol. 44, No. 4, 2006, pp. 687-697.

Shih, T.-H., and Liu, N.-S., "A non-linear Dynamic Subscale Model for Partially Resolved Numerical Simulation (PRNS)/Very Large Eddy Simulation (VLES) of Internal Non-Reacting Flows," NASA/TM-2010-216323, May 2010.

M.S. Raju, EUPDF-II: "An Eulerian Joint Scalar Monte Carlo PDF Module Users' Manual," NASA/CR-2004-213073.

Shih, T.-H., "Constitutive Relations and Realizability of Single-Point Turbulence Closures" Turbulence and Transition Modeling, Chapter 4., Edited by Hallback, M., Henningson, D.S., Johansson, A.V. and Alfredsson, P.H., KLUWER ACADEMIC PUBLISHERS, 1996.

Shih, T.-H., Zhu, J., Liou, W., Chen, K.-H., Liu, N.-S. and Lumley, J. L., " Modeling of Turbulent Swirling Flows," NASA/TM-1997-113112, 1997.

Shih, T.-H., "Some developments in computational modeling of turbulent flows," Fluid Dynamic Research 20 (1997) 67-96.

Ryder, R. C., "Application of the National Combustion Code towards Unsteady Mixing and Combustion Modeling," AIAA-2000-0335, January 2000.